C. Boit, H. Lohrke , P. Scholz, A. Beyreuther , U. Kerst , Y. Iwaki

Contactless visible light probing for nanoscale ICs through 10 µm bulk silicon

Conference Object, Published Version
This version is available at http://dx.doi.org/10.14279/depositonce-5949.

Suggested Citation
Boit, C. et al: Contactless visible light probing for nanoscale ICs through 10 µm bulk silicon. - In: Proceedings of the 35th Annual NANO Testing Symposium (NANOTS2015). - Osaka: Institute of NANO Testing, 2015. - pp. 215–221

Terms of Use
Copright applies. A non-exclusive, nontransferable and limited right to use is granted. This document is intended solely for personal, non-commercial use.

WISSEN IM ZENTRUM UNIVERSITÄTSBIBLIOTHEK

Technische Universität Berlin

Contactless Visible Light Probing for Nanoscale ICs through 10 µm Bulk Silicon

C. Boit[a], H. Lohrke[a], P. Scholz[a], A. Beyreuther[a], U. Kerst[a], Y. Iwaki[b]

[a] Dept. Semiconductor Devices, TUB - Berlin Univ. of Technology, Germany
[b] Hamamatsu Photonics GmbH, Germany

Abstract: This paper explains why only optical techniques will be able to provide debug and diagnosis of bulk silicon FinFET technologies. In order to apply optical techniques through a convenient thickness of silicon on the one hand, light is limited to NIR to minimize absorption. To match resolution requirements on the other hand, it becomes mandatory to use shorter wavelengths. Two key issues have to be addressed: First, the penetration depth of visible light is only a few µm. This challenges device preparation and integrity. Our approach makes use of confocal microscopy suppressing back surface reflection and thus relaxing the preparation requirements to around 10 µm. Second, only solid immersion lenses (SIL) enable nanoscale resolution. But instead of silicon, materials transparent to visible light and providing a high refractive index are necessary. Our concept is based on 658 nm/633 nm laser and supports GaP as SIL material. We demonstrate the power of confocal imaging and prove contactless probing through a device thickness of 10 µm. We discuss how confocal optics relax the thickness requirements for visible light imaging and probing and we layout the concept for a GaP SIL. This concept opens the path to the design of nanoscale visible light debug and diagnosis.

Keywords: EOP, EOFM, LVP, LVI, visible light LVP, nanoscale IC debug & diagnosis, low power IC debug & diagnosis, confocal microscopy, backside failure analysis, SIL, bulk Si FinFET failure analysis, bulk Si FinFET debug & diagnosis

1. Introduction

The ITRS roadmap has predicted in the first decade of this millennium nanoscale transistor technologies on SOI wafers with ultra-thin silicon (UTS) towards 20 nm thickness for fully depleted (FD) FETs [1]. Under this impression, IC debug and diagnosis seemed to be naturally focused on the easy endpoint of removing the buried oxide (BOX) chemically and having the back surface carry the logical information of each node, isolated from the others. Many surface-sensitive, highly resolving techniques like scanning probes, near field optics or e-beam probing seemed to be the proper debug answers to the nanoscale device dimensions in the UTS approach [2].

A few years later, FinFETs offer FD condition just by the small width of the vertical fin, so no UTS would be required anymore to create an FD FET.

Now, IC debug and diagnosis for bulk Si FinFET technologies had to find a new way to increase feature resolution. To that point, near infrared (NIR) optical techniques (photon emission, laser stimulation, electro-optical probing) have been established with wavelengths around 1 µm, allowing to pass through several hundred µm of bulk silicon. Resolution is then limited to identify nodes of 120 nm technologies, 90 nm or even 60 nm only with uncertainty. As a result, solid immersion lenses (SIL) have been introduced increasing the NIR resolution by the index of refraction, 3.5 for a silicon SIL. This extends the application of optical techniques to technologies of around 20 nm feature size. However, if we were able to just expand the spectrum to visible light, we would increase resolution by another 2x [3], good enough for current and near future FinFET technologies around 10 nm. This paper explores how much effort it takes to gain resolution using smaller wavelengths. The presented study investigates electro-optical probing, the debug

Contact author: christian.boit@tu-berlin.de

 ©ナノテスティング学会

technique of highest potential for low power telecommunication technologies.

2. Why Confocal Microscopy?

Confocal microscopy gives an important advantage when we want to achieve the best possible tradeoff between highest resolution by applying shorter wavelengths with very short absorption ranges and a large thickness of the bulk silicon. This allows for a simpler sample preparation and gives better mechanical stability, e.g. for SIL placement.

2.1. Confocal Microscopy Basics

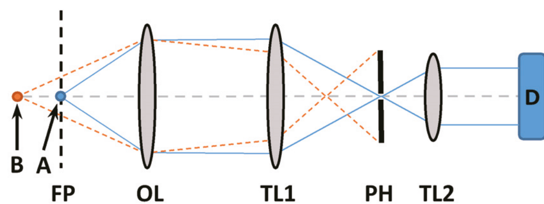

Figure 1: Simplified confocal detector. See text for abbrev.

Figure 1 depicts a simplified confocal detector setup. The light from the focal plane FP, inside the device under test, is converted into a parallel beam by the objective lens OL. This light converges onto a second focus inside a telescope built of the two telescope lenses TL1 and TL2. After the light has passed the telescope it will hit the detector D. Inside the telescope is the most important component of the confocal setup: the pinhole PH which has a very small diameter. This pinhole is placed exactly in the focal plane of the two telescope lenses TL1 and TL2. Light from point A can pass the pinhole PH without any attenuation, as its focal point is exactly at the pinhole. Light from point B will be focused outside of the pinhole and so a large quantity will be blocked by the pinhole. For that reason, the signal from point B will be much weaker than the signal from point A. If this setup is extended by scanning the beam and by adding a laser source for illumination, we have the setup for a classical confocal laser scanning microscope. This microscope will then be able to analyze the signal of not only a spot, but from the whole 2D focal plane. It will mainly pick up light from the focal plane and strongly suppress signals coming from other planes.

2.2. Benefits of Confocal Microscopy

To see why it is advantageous to use a confocal setup for visible light imaging and probing applications one has to take a look at the basic configuration of visible light (VIS) imaging/probing as compared to near-infrared (NIR) imaging/probing.

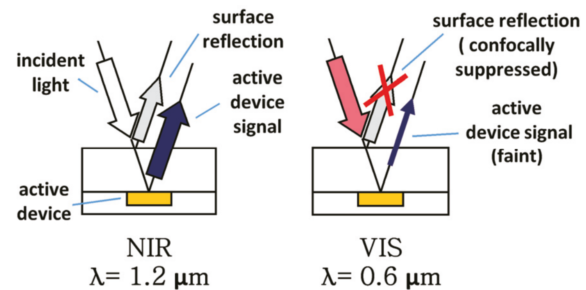

Figure 2: Comparison of expected NIR and VIS signal configurations.

On the left side of Figure 2 NIR backside illumination of a silicon device is depicted. Since the absorption in the silicon substrate is relatively low for NIR, the light reflected from the active device is relatively strong compared to the reflection from the back surface. If we now consider the case of VIS illumination as on the right side of Figure 2 we can see that due to the increased absorption the signal reflected from the active device becomes very faint. This signal is much harder to detect, and there is a lot of light from the back surface reflection entering the optics, which contains no information about the device operation. The comparatively large back surface reflection signal might even lead to saturation of the detector which might keep us from successfully performing such a measurement at all. If we use confocal optics we can expect the signal from the back surface to be strongly suppressed (red “X” in Figure 2), enabling us to perform measurements on the faint light signal from the active device.

Figure 3 shows a comparison of the behavior of the surface reflection in the case of a conventional microscope (dashed line) and in the case of a confocal microscope (dotted line) [4].

 ©ナノテスティング学会

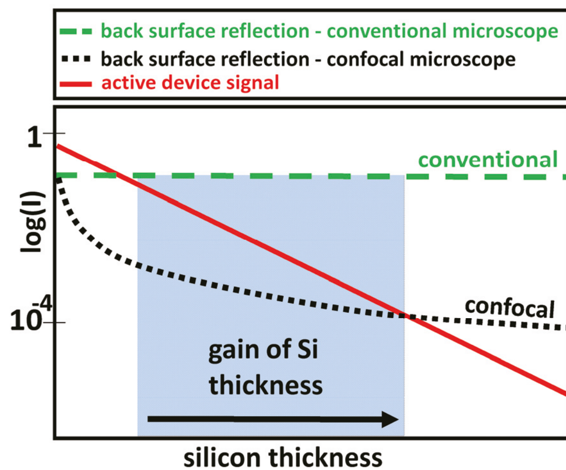

Figure 3: Gain of Si thickness with confocal setup: comparison of back surface reflection with conventional and confocal microscopy.

The active device signal (full line) decreases exponentially with the thickness of the bulk silicon according to the Beer-Lambert law. We observe a drastic reduction of the surface reflection in the confocal setup. When comparing the points where the intensity of the active device signal equals the intensity of the surface reflection, it becomes apparent why the confocal setup enables us to work with considerably thicker silicon without losing signal quality. These relaxed thickness requirements entail several advantages: facilitation of device preparation with a higher yield, as well as improvement of mechanical stability, beneficial e.g. for SIL placement.

3. Experiments

We designed our experiments component by component. This is helping us to work on improving the resolution by shortening the wavelength even without a SIL. For this, we first present visible light imaging results with improved resolution. Then, we show a proof of concept for visible light optical probing. Our VIS-SIL concept will be presented in a separate chapter.

3.1. Devices and Sample Preparation

Device selection for our investigation can be quite simple. As the improvement of visible over NIR light microscopy is independent of SIL optics, we can separate this part from SIL investigation.

In that case, a 60 nm technology is well suited to see the advantage of visible light optical imaging compared to NIR imaging, even without a SIL. Therefore we picked Altera Cyclone IV FPGAs (60 nm technology) for metal pattern imaging experiments.

The key question for electro-optical probing measurements has been signal strength through the moderate bulk thickness. In that case, feature size is of minor priority. With a larger scale device, the different interactions in pn junctions and gates can be studied separately. For that purpose we used an Infineon FET test structure (120 nm technology), similar to the one used in [5].

We thinned the devices to remaining bulk Si thicknesses of 10 µm to 30 µm using an ULTRA TEC “ASAP-1”. The Infineon test structures were mounted into AMCOR BGA packages and bonded at TU Berlin.

3.2. Experimental Setup

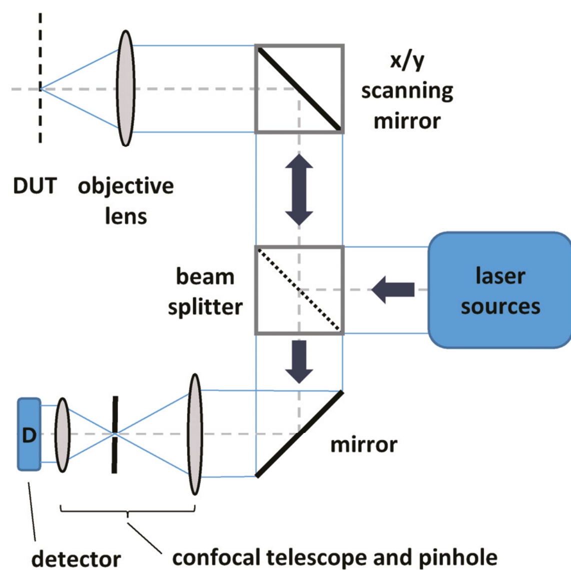

Figure 4: Simplified confocal LSM setup.

We designed our visible light imaging/probing experiments using confocal laser scanning microscopy (see chapter 2). We used two identical commercial confocal LSMs from Zeiss, model “LSM 21/31 IR”. The simplified optical setup of these microscopes is depicted in Figure 4.

The microscopes contain the usual microscope optics, an x/y galvanometric scanner, the confocal telescope and pinhole and a photomultiplier tube (PMT) detector.

The first microscope, which was used for imaging experiments already contained a 633 nm helium-neon laser with 15 mW power and had a 1 mW 1.15 µm helium-neon laser added externally.

The microscope is equipped with a germanium diode for NIR detection and therefore the VIS and NIR imaging experiments could be conducted with the original Zeiss software already installed.

The second microscope, which was used for probing experiments, was equipped with a 100 mW 658 nm diode laser instead of the standard helium-neon laser. The signal of the internal photomultiplier tube (PMT) detector of this microscope was tapped after the built-in amplification circuit and then fed into a Stanford Research Systems “SR844 RF” lock-in amplifier and into a LeCroy “WavePro 735 Zi” oscilloscope. The lock-in amplifier could then be used for the initial adjustments and the oscilloscope for the capturing of the final probing waveform. A Keithley “3390” pulse generator was used to supply the device with electrical signals.

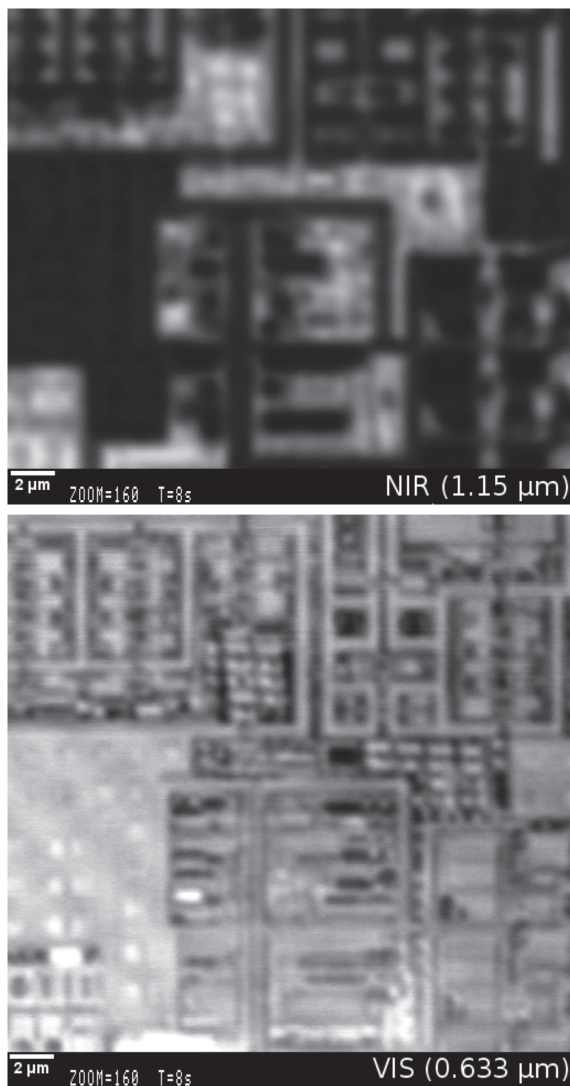

Figure 5: Comparison of NIR 1.15 µm and VIS 0.633 µm backside pattern images.

3.3. Imaging Experiments

The imaging experiments were conducted with the dual wavelength LSM. For initial tests we used Cyclone IV devices which were thinned to a target value of 10 µm, 20 µm and 30 µm remaining silicon thickness. For 30 µm we were not able to get any pattern images, for 20 µm there was a very faint and noisy signal and for 10 µm we were able to get good pattern images. We therefore continued our experiments with the 10 µm sample only. We then measured the position difference in the focusing z-axis between focusing on the back surface and on the pattern image with the NIR laser in confocal mode. Using the refractive index, we could determine the actual thickness to be 10.2 µm. Then, we took pattern images of the same location using 1.15 µm (NIR) and 633 nm (VIS) laser wavelengths. The resulting images can be seen in Figure 5.

The VIS image contains evidently much more detail. Some parts of the image showed a contrast inversion compared to the 1.15 µm laser image, probably due to interference effects.

A rough estimate of the improvement in resolution can be derived from edges in line scans fitted in the NIR and VIS images. We used an error function for the fit following an approach by [6].

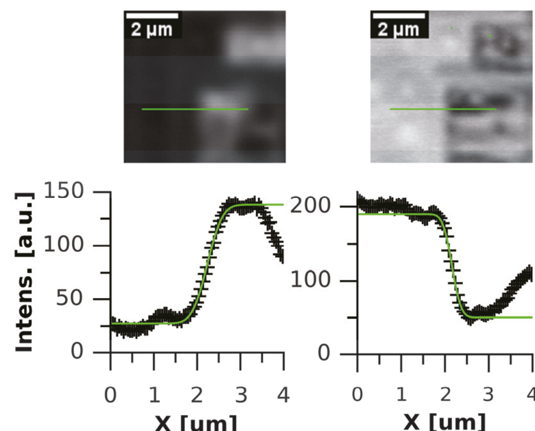

Figure 6: Line plots and fitted error functions through dark-bright transition edges in the NIR (left) and VIS (right) pattern images. The fit shows an improvement by a factor of 1.68x.

The location of the line plots and the resulting fits can be seen in Figure 6. We fitted the error function only in the transition region to minimize the influence of underlying structures and fill shapes in the plateau regions. The detailed fitting

function and parameter table is described in the appendix.

This fit indicates an improvement of 1.68x which explains the impressively increased image quality. The fit result is also very close the theoretically expected 1.82x improvement because of the reduced wavelength (1.15 µm vs. 0.633 µm).

3.4. Electro-Optical Probing Experiments

For the probing experiments the 658 nm 100 mW high power LSM was used. We used the Infineon 120 nm technology 1.2 V test structures which were thinned to a target thickness of 10 µm. The actual thickness was measured by confocal focusing and was 10.9 µm. We used large area PFET structures for testing our probing setup. The gate was driven by a 26 kHz square wave signal of -1.5 V amplitude from a clock generator. All other contacts were connected to ground. The laser was pointed into the gate area. The measurement has been performed by averaging 1.000.000 waveform traces with the connected oscilloscope to eliminate noise. The oscilloscope was synchronized to the gate signal by using a +1.65 V synchronization signal supplied by the clock generator. The resulting probing waveform can be seen in Figure 7.

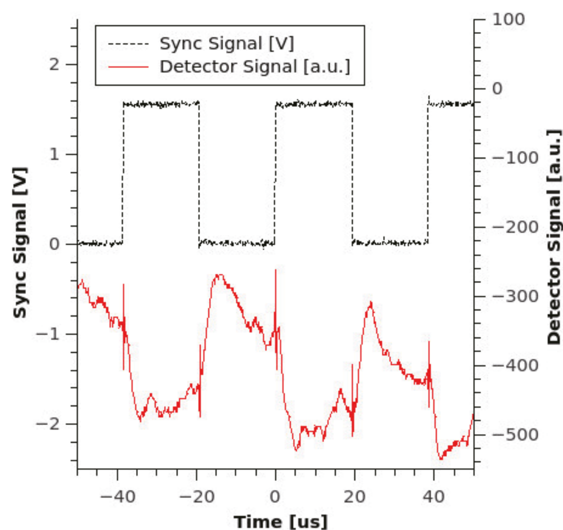

Figure 7: Averaged detector signal for a 26 kHz -1.5 V low/ 0 V high square wave applied to the gate. The measurement was averaged for 1.000.000 traces using the 1.65 V sync signal supplied by the clock generator. The laser is pointed into the gate area.

The results show that the detector waveform is corresponding to the clock generator synchronization output. The waveform still contains some noise and crosstalk from switching is also visible, nevertheless the clock signal is clearly detectable. We also evaluated other forms of stimulation like pulsing the drain, however this resulted in smaller signals which would require a longer integration time.

4. SIL for Visible Light

The use of a solid immersion lens (SIL) is expected to bring further improvement in resolution, beyond the previously presented results. SILs are well established in debug & diagnosis. Today, silicon SILs for NIR techniques with an *NA* of up to 3.1 (NanoLens-SHR [7]) are part of commercially available tools. Hamamatsu claims a resolution of around 120 nm with such a machine. Adapting the SIL technique to VIS at about half the wavelength could bring a resolution close to 60 nm within reach, based on the previous statement. With a given technology node needing about 6-8 times its value in resolution for optical analysis, this could enable optical analysis of the 10 nm technology node and possibly beyond.

The benefit of a SIL can be explained by looking at the definition of optical resolution, e.g. according to Abbe as

$$R = \lambda / (2\,NA). \qquad (1)$$

The main components herein are the wavelength λ and the numerical aperture *NA*. A key aspect of this work is to use visible light at 633 nm and 658 nm wavelength (see chapter 3.2). Therefore the common feature of immersion microscopy needs to be applied for additional enhancement: Increasing the *NA*. The index of refraction n and the opening angle β create *NA* by

$$NA = n \sin\beta. \qquad (2)$$

For regular microscopy in air n is usually omitted due to $n_{air} = 1$. Looking at microscopy in air applied to the backside analysis through silicon bulk material shows the need for SILs (Figure 8). Without immersion techniques the benefit of the high index refraction material is defeated by total internal refraction and a resulting poor maximum

©ナノテスティング学会

opening angle β_{1max} (3) derived from Snell's law (4).

$$\beta_{1max} = \arcsin(n_2/n_1), \text{ with } \beta_2 = 90° \quad (3)$$
$$n_1 \sin\beta_1 = n_2 \sin\beta_2 \quad (4)$$

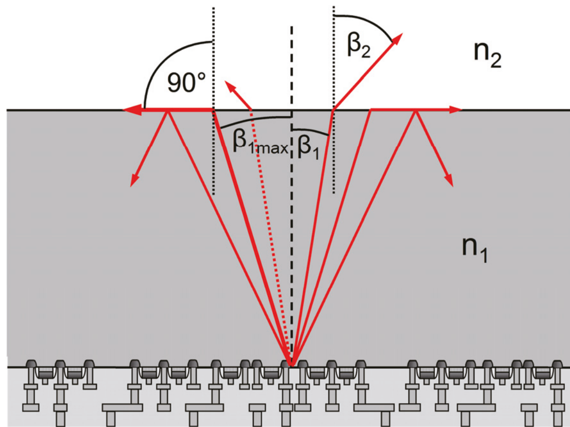

Figure 8: Refraction at the silicon interface.

With a visible wavelength of e.g. 658 nm β_{1max} is at merely 15,1°. This limiting refraction at the interface can be reduced or entirely avoided by a SIL (Figure 9), leading to an improvement in opening angle, *NA* and thereby also in resolution. While the best match for NIR analysis of a silicon sample is a silicon SIL, this can not be applied for visible light analysis. The strong absorption of silicon at e.g. 658 nm wavelength creates the need for moderately thin bulk silicon and a different "new" SIL material with low absorption for visible light. While the bulk material can be thinned within reason (see chapters 3.3, 3.4), the SIL itself needs to be sufficiently large to allow for reliable production and handling.

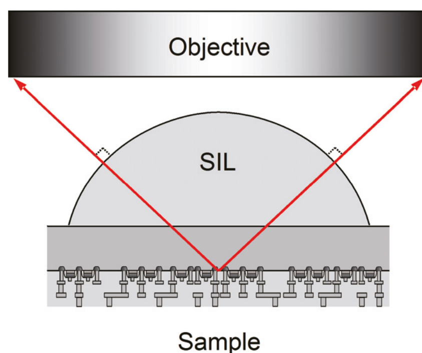

Figure 9: Simplified concept of a central SIL.

Requirements for the "new" SIL material include an index of refraction n close to that of bulk silicon to enable a large opening angle β_{1max}, and low absorption to efficiently pass light through several hundred µm of material. A comparison of semiconductor and other lens materials (Table 1) indicates that the best choice is Gallium Phosphide (GaP). With n = 3.3 at 658 nm wavelength, it offers a maximum opening angle β_{1max} of 59.0° at the GaP-Si interface (compared to 15,1° for air-Si) and an improvement in resolution equal to the index of refraction by 3.3.

Current research [8] shows that an ultra high precision (UHP) computer numerical controlled (CNC) milling/turning machine will successfully create a GaP SIL and make it available to the authors in the near future. Another possible method is to use a focused ion beam for lens shaping [9, 10], which will also be considered. In either case an additional improvement in optical resolution by a factor of up to 3.3 with a GaP SIL is within reach.

Table 1: Material properties at 658 nm wavelength.

Material	n	W_g (300 K)
Si	3.84 [12]	1.12 eV [11]
GaP	3.29 [12]	2.25 eV [11]
SiC	2.63 [13]	2.36-3.03 eV
C	2.41 [14]	5.46–6.4 eV
S-LAH79 Glass	1.99 [15]	-

5. Conclusions

We presented a concept for designing optical debug and diagnosis techniques using photon energies much higher than the semiconductor bandgap. We demonstrated for bulk Si that the optical resolution is really increased by the expected margin (in our case for 633 nm an improvement by roughly 2x). We presented the advantage of using high level confocal optics for suppression of back surface reflection, which helps us to expand the maximum device thickness to 10 µm. For such a relaxed thickness, device preparation requirements are not overly hard and SIL operation should not be problematic from a mechanical stability point of view. The presented concept of a SIL for visible light is realistic and flexible for use of other wavelengths as well. The

©ナノテスティング学会

presented results show the feasibility to design visible light techniques for nanoscale IC debug and diagnosis to the resolution requirements of feature sizes down to 10 nm and lower.

Acknowledgements

The authors would like to thank Andreas Eckert for device preparation and Rene Hartmann for bonding, both TU Berlin, Germany. We would also like to thank Enrico Dietz, also TU Berlin, for very fruitful discussions concerning the detection scheme. Heiko Lohrke is supported by the Helmholtz Research School on Security Technologies.

References

[1] ITRS - International Technology Roadmap for Semiconductors, http://www.itrs.net/reports.html

[2] C. Boit, R. Schlangen, U. Kerst, and T. Lundquist, “Physical Techniques for Chip-Backside IC Debug in Nanotechnologies,” IEEE Design & Test of Computers - Special Issue on Silicon Debug and Diagnosis, 25, pp. 250-257, 2008.

[3] J. Beutler, J. Clement, M. Miller, J. Stevens, and E. Cole, “Visible Light LVP on Ultra-Thinned Substrates,” International Symposium for Testing and Failure Analysis (ISTFA), 2014.

[4] T. Wilson, “Confocal Microscopy,” Academic Press Inc., San Diego, pp. 7 – 60, 1990.

[5] U. Kindereit, G. Woods, J. Tian, U. Kerst, R. Leihkauf, and C. Boit, “Quantitative investigation of laser beam modulation in electrically active devices as used in laser voltage probing,” IEEE Transactions on Device and Materials Reliability, vol.7 no.1, pp. 19-30, 2007.

[6] S. Ippolito, “High Spatial Resolution Subsurface Microscopy,” Boston University, 2004.

[7] Hamamatsu NanoLens https://www.hamamatsu.com/resources/pdf/sys/SSMS0053E_Nanolens-SHR.pdf

[8] J. Vaclavík, R. Doleèek, V. Lédl, and P. Psota, “Experimental study on SPDT machining of Gallium Phosphide,” Proc. SPIE 8884, Optifab 2013, 2013.

[9] P. Scholz, N. Herfurth, M. Sadowski, T. Lundquist, U.Kerst, and C. Boit, “Efficient and flexible Focused Ion Beam micromachining of Solid Immersion Lenses in various bulk semiconductor materials – An adaptive calibration algorithm,” Microelectron. Reliab., pp. 7–10, 2014.

[10] P. Scholz, M. Sadowski, S. Kupijai, M. Henniges, C. Theiss, S. Meister, D. Stolarek, H. Richter, M. Boostandoost and C. Boit, “Turning sample into (re)solution: Focused Ion Beam shaped Solid Immersion Lenses,” International Symposium for Testing and Failure Analysis (ISTFA), 2015.

[11] C. Kittel, “Introduction to Solid State Physics,” 6th Ed., New York: John Wiley, p. 185, 1986.

[12] D. Aspnes and A. Studna, “Dielectric functions and optical parameters of Si, Ge, GaP, GaAs, GaSb, InP, InAs, and InSb from 1.5 to 6.0 eV,” Phys. Rev. B 27, 985-1009, 1983.

[13] S. Singh, J. R. Potopowicz, L. G. Van Uitert, and S. H. Wemple, “Nonlinear optical properties of hexagonal silicon carbide,” Appl. Phys. Lett. 19, 53, 1971.

[14] F. Peter, “Über Brechungsindizes und Absorptions-konstanten des Diamanten zwischen .226 und .644 µm,” Zeitschrift für Physik 15, 358-368, 1923.

[15] Ohara Glass Catalog Data http://www.oharacorp.com/catalog.html

Appendix A: Fitting function

The fitting function used in chapter 3.3 was of the following type:

$$Y = y_0 + A\ (\mathrm{erf}((x\text{-}x_0)s) + 1)\ /\ 2 \qquad (5)$$

This function expresses the line plot grayscale value Y with the following parameters: A is the grayscale level of the bright edge, y_0 is the level of the dark edge, x_0 is the position of the edge transition and s is the scaling factor of the function. The resulting fit parameters can be found in Table 2. The parameter s that is connected to resolution improvement changes from 2.57 to -4.31 when switching from NIR to VIS. The change in sign originates from the contrast inversion mentioned in chapter 3.3. The ratio of the two scaling factors is therefore 1.68.

Table 2: Line plot fitting results.

NIR-Fit		**VIS-Fit**	
A	110,61	A	139,73
s	2,57	s	-4,31
x_0	2,23	x_0	2,16
y_0	27,42	y_0	50,10